ISSN 1560-0904, Polymer Science, Series B, 2020, Vol. 62, No. 2, pp. 163–168. © Pleiades Publishing, Ltd., 2020.

COMPOSITES

Fabrication and Characterization of Poly(aniline-*co*-4-bromoaniline)/Clay Nanocomposite

N. El-hoda. Bouabida[a], A. Hachemaoui[a], A. Yahiaoui[a], H. Gherras[a], A. Belfedal[b], A. Dehbi[c,*], and Abdel-Hamid I. Mourad[d]

[a] *Laboratoire de chimie Organique, Macromoléculaire et des Matériaux (LCOMM), Université de Mascara, Faculté des Sciences Exactes, BP 763 Mascara, 29000 Algeria*

[b] *Laboratoire de Chimie Physique des Macromolécules et Interfaces Biologiques, Université de Mascara Algeria, City, Algeria*

[c] *Engineering Physics Laboratory, University Ibn Khaldoun, Zaaroura, Tiaret, 14000 Algeria*

[d] *Mechanical Engineering Department, College of Engineering, United Arab Emirates University, Al-Ain, United Arab Emirates*

**e-mail: abddehbi@gmail.com*

Received July 13, 2019; revised November 20, 2019; accepted November 30, 2019

Abstract—Poly(aniline-*co*-4-bromoaniline) nanocomposites were prepared via in situ polymerization in different molar ratio in the presence of Cu^{2+}–monmorillonite. The X-ray diffraction confirmed that the basal space of Cu^{2+}–montmorillonite increased after the organophilization. Poly(aniline-*co*-4-bromoaniline)/Cu^{2+}–monmorillonite nanocomposites were prepared by intercalating of aniline and 4-bromoaniline with treated organically layers of Cu^{2+}–monmorillonite following by polymerization initiated by ammonium peroxdisulfate. The nanocomposites were characterized by FTIR, XRD, and UV–Vis spectroscopy.

DOI: 10.1134/S1560090420020013

INTRODUCTION

Recently, the conducting polymer materials have attracted great interest in technological and electrical applications, such as in rechargeable batteries [1], redox capacitors, electromagnetic shielding devices [2], solar cells [3–5], microelectronic devices [6, 7] and sensors [8–11] due to their chemical and physical properties. Their conductivity is generally similar to that of metals and inorganic semiconductors [12, 13].

Among the conducting polymers, polyanilines have become one of the most attractive conducting polymers due to high stability, easy availability of raw materials, simple and easy methods of synthesis [14, 15], economical efficiency [16]. Furthermore, the electrical properties can be controlled by the oxidation and protonation state [17–19]. PANI is either insulating or electrically conductive, depending on the oxidation state and protonation level. Only in the intermediate oxidation state, the protonated emeraldine form is conductive (Scheme 1). The fully reduced leucoemeraldine and oxidized pernigraniline are insulating materials [20]. Various methods of preparation, characterizations and current commercial applications of PANI are summarized in [21–27].

In this paper, we focus on the synthesis of nanocomposites based on polyaniline and poly(aniline-*co*-4-bromoaniline) and Cu^{2+}–monmorillonite via *in situ* polymerization of aniline and/or 4-bromoaniline onto Cu^{2+}–monmorillonite nanoparticles.

EXPERIMENTAL

4-Bromoaniline (4-BAN) and aniline (ANI) were purchased from Aldrich, ammonium peroxdisulfate (APS), $CuSO_4$ aqueous solution were used as modification of montmorillonite (M-Cu^{2+}). The water used for the preparation of the solutions was obtained from an Elga lab water Purelab Ultra system. The montmorillonite clay called Maghnite obtained from western of Algeria has been used.

The clay which has been used is supplied by a local company known as ENOF Maghnia (western of Algeria). The clay sample is formed in cuprous form by ion exchange with a solution of $CuSO_4$ (1M) with stinging for 24 h. After the modification, the troublesome SO_4^{-2} ions are removed by washing with distilled water, the M-Cu^{2+} is dried at 105°C in an oven and then stored.

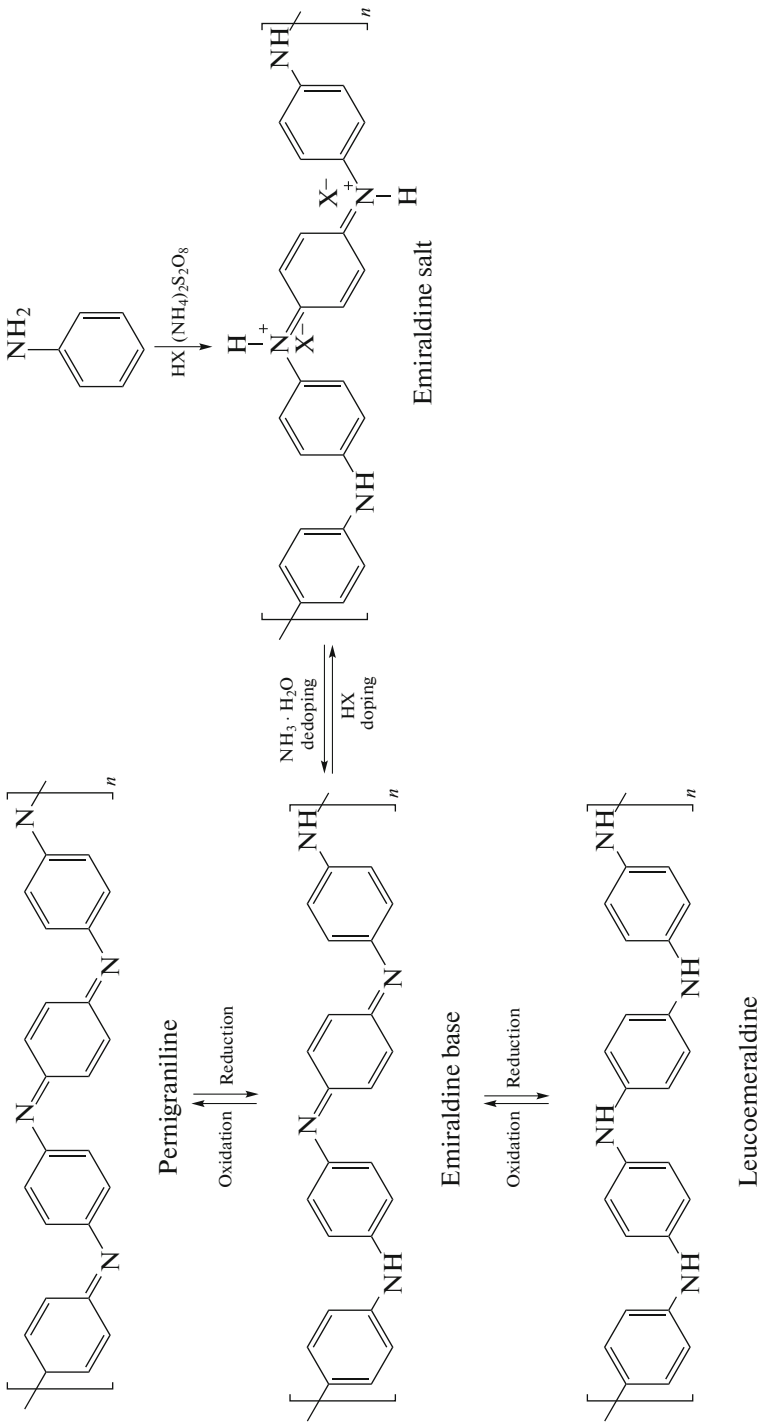
HX
$(NH_4)_2S_2O_8$
Emiraldine salt
$NH_3 \cdot H_2O$ dedoping
HX doping
Pernigraniline
Oxidation
Reduction
Emiraldine base
Oxidation
Reduction
Leucoemeraldine

Scheme 1.

Table 1. Elementary compositions of raw Maghnite and M-Cu^{2+} clays

Sample	SiO_2	Al_2O_3	Fe_2O_3	CaO	MgO	Na_2O	K_2O	TIO_2	CuO	Pert in fire
Raw-Maghnite	67.7	24.1	2.8	0.01	3.8	0.01	1.3	0.2	–	0.56
M-Cu^{++}	74.0	17.2	1.8	–	2.6	–	2.0	0.1	2.1	0.20

The composition of M-$Cu^{2+}$was measured by X-ray fluorescence (Table 1).

A quantity of the ANI and 4-BAN (4-BAN : ANI = 100 : 0, 50 : 50, 80 : 20, and 20 : 80) is mixed with 0.25 g of cuprous clay for 2 min by magnetic stirring at room temperature. After that, 100 mL of distilled water is added while keeping the mixture under magnetic stirring at room temperature for 2 h. The polymerization begins with the addition of 0.5 g of initiator $(NH_4)_2S_2O_8$. The reaction was conducted during 24 h. The solid product is filtered, then washed with distilled water and dried in an oven at 105°C.

The UV–Vis absorption spectra were registered in NMP. Fourier transforms infrared (FTIR) spectroscopy was recorded using a Bruker Alpha. For the X-ray diffraction**,** the powder nanocomposites were taken using Bruker CCD Apex equipment with an X-ray generator (Cuka and Ni filter) operated at 40 kV and 40 Ma.

RESULTS AND DISCUSSION

The FTIR spectra reveal the different absorption bands resulting from the formation of the nanocomposite (Fig. 1, Table 2). In the spectra of P(4-BANI)/M-Cu^{2+} and P(ANI-*co*-4-BAN)/M-Cu^{2+} the appearance of a local deformation band between 3597 and 3606 cm^{-1} can be attributed to the free N–H stretching vibration and hydrogen bonded N–H between amine and imines sites [28, 29]. An elongation band with an average intensity between 3230 and 3240 cm^{-1} of the C=N bond is associated with vibrations of quinine diimines. An elongation band of low intensity is situated between 1561 and 1570 cm^{-1} of the –C=C bond of the benzene diamine group. An elongation band of low intensity of the C–H bond is located at 818 cm^{-1}. The bands situated respectively at 452 and 521 cm^{-1} of the Si–O and Al–OH bonds are connected with the M–Cu^{2+}, which confirms the presence of the two organic/inorganic phases [30–33].

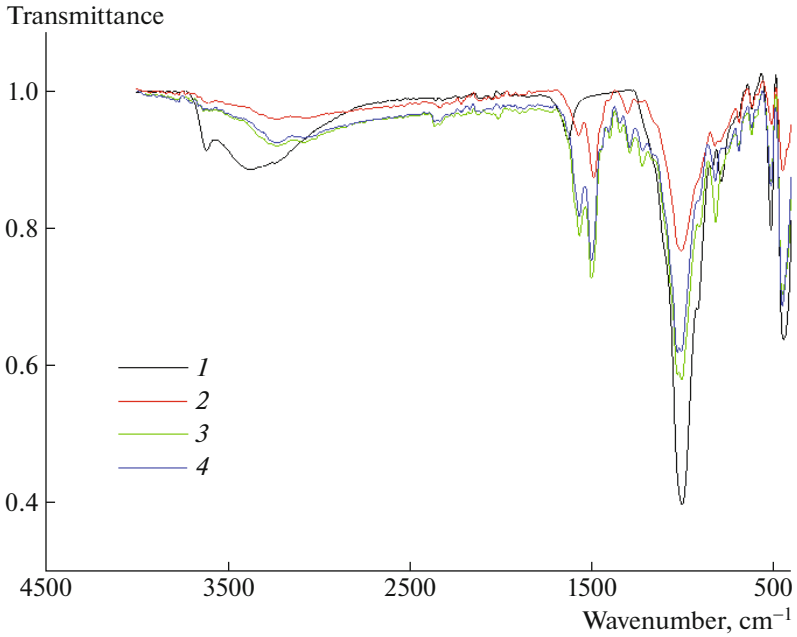

Fig. 1. (Color online) FTIR absorption spectra of the (*1*) P(4-BAN), (*2*) P(ANI-*co*-4-BAN)/M-Cu^{2+} (80/20), (*3*) P(ANI-*co*-4-BAN)/M-Cu^{2+} (20/80), (*4*) P(ANI-*co*-4-BAN)/M-Cu^{2+} (50/50).

Table 2. Characteristic FTIR band absorption frequencies of P(4-BAN) and P(ANI-*co*-4-BAN)

Assignments	Wavenumbers, cm^{-1}			
	P(4-BAN)	P(ANI-*co*-4-BAN)		
		80/20	20/80	50/50
N–H	3606	3600	3600	3597
Bromure substituents	3240	3231	3230	3231
–C–H	818	818	818	818
–C=C	1561	1570	1570	1561
–C–N	1490	1490	1490	1490

Figure 2 shows the optical measurements of polymers at room temperature in UV–Vis region. The spectra were obtained after dissolving the P(ANI-*co*-4-BAN)/M-Cu^{2+} (50/50) in NMP [34] reveal two absorption peaks located at 242 and 351 nm, which are attributed to π–π* transition of the benzenoid ring and *n*–π* transition of benzenoid to quinoid, respectively [35].

The UV–Vis spectra of P(4-BAN) present absorption peaks at 238 and 345 nm assigned to π–π* and *n*–π* respectively. P(ANI-*co*-4-BAN)/M-Cu^{2+} (20/80) has two characterization absorption bands show at 240 and 350 nm which are attributed to π–π* transition of the benzenoid ring and *n*–π* transition of benzenoid to quinoid, respectively. For P(ANI-*co*-4-BAN)/M-Cu^{2+} (80/20) the bands were observed at 215 and 356 nm; these results indicate the presence of electrons with drawing group in the polymer.

The XRD has often been used for determining the degree of intercalation and/or exfoliation of clay in the polymer matrix [36]. The intercalation of poly(4-BAN) and poly(ANI-*co*-4-BAN) occurs inside a MMT interlayer as shown in Fig. 3 and Table 3.

The *d*-spacing values (d001) were calculated from the peak position of XRD pattern using Bragg's equation $d = 2\pi/q$, where q is the magnitude of scattering vector defined as $q = (4\pi/\lambda)\sin(\theta)$, where λ is the X-ray wavelength and 2θ is the scattering angle [37]. The introduction of the polymers had considerable effect on the diffraction pattern.

The nanocomposites have an intercalated structure, since the diffraction peaks of the charge are observed in Fig. 3. Its value ranges from 12.7960 Å for M-Cu^{2+} to 14.5695 Å for P(4-BAN)/M-Cu^{2+}, 15.0980 Å for P(ANI-*co*-4-BANI)/M-Cu^{2+} (20/80), 15.2324 Å for P(ANI-*co*-4-BANI)/M-Cu^{2+} (80/20), and 15.3081Å for P(ANI-*co*-4-BANI)/M-Cu^{2+} (50/50).

The increase of the interlamellar space corresponds to a diffusion of the P(ANI-*co*-4-BAN) chains and can be interpreted by a greater active interaction for that of P(ANI-*co*-4-BAN) between the polymer and

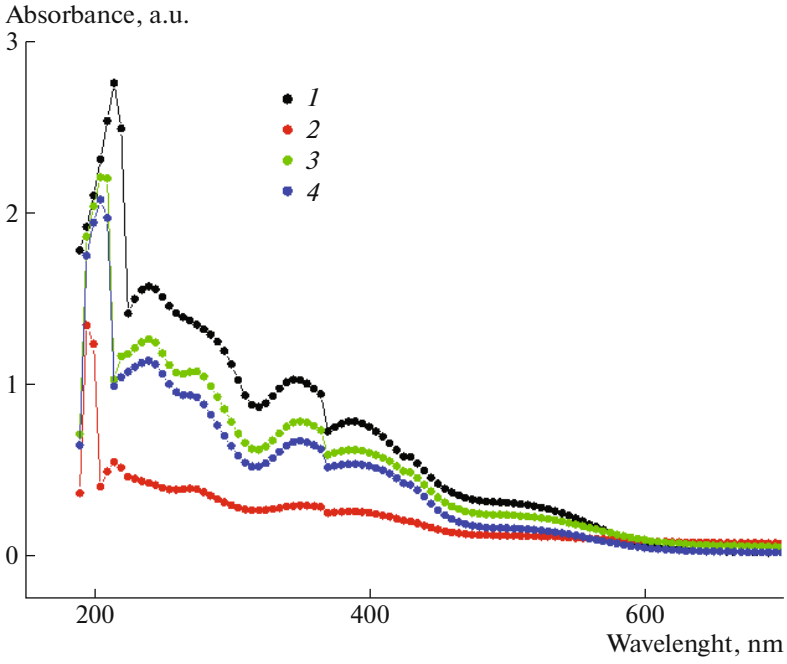

Fig. 2. (Color online) UV–Vis spectra of the (*1*) P(4-BAN), (*2*) P(ANI-*co*-4-BAN)/M-Cu^{2+} (80/20), (*3*) P(ANI-*co*-4-BAN)/M-Cu^{2+} (20/80), (*4*) P(ANI-*co*-4-BAN)/M-Cu^{2+} (50/50).

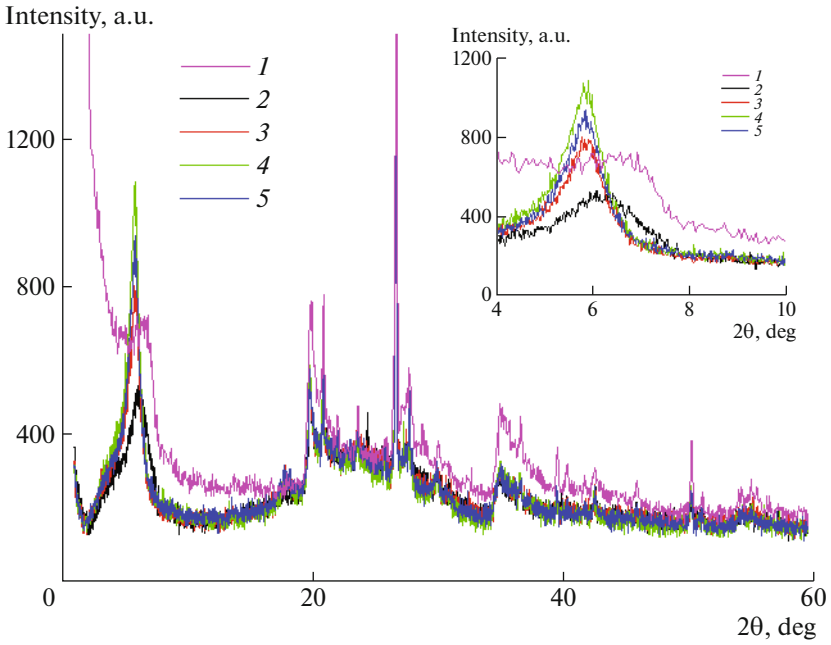

Fig. 3. (Color online) The X-ray diffraction (XRD) measurement of (*1*) M-Cu^{2+}, (*2*) P(4-BAN)/M-Cu^{2+}, (*3*) P(ANI-*co*-4-BAN)/M-Cu^{2+} (50/50), (*4*) P(ANI-*co*-4-BAN)/M-Cu^{2+} (20/80), (*5*) P(ANI-*co*-4-BAN)/M-Cu^{2+} (80/20).

the hybrid charge. It should be noted that this dilation of the lamellar structure cannot be explained by the polymerization of the 4-BAN, this process being accompanied rather by a narrowing of the interlamellar distance.

The electrical measurements of polymers P(4-BAN), P(ANI-*co*-4-BAN)/M-Cu^{2+} (80/20), P(ANI-*co*-4-BAN)/M-Cu^{2+} (20/80), P(ANI-*co*-4-BAN)/M-Cu^{2+} (50/50) were performed with Four-Electrode measurement at room temperature. The results are summarized in the Table 4. The electrical conductivity of the different copolymers at room temperature depends on the chemical composition, morphology, the amorphous nature of the copolymer and the degree of doping of the specific polymer as well as electronic and steric factors. These results show that the electrical conductivity of the resultant copolymers increase with increasing the percentage of M-Cu^{2+}, with electrical conductivity values for the copolymers in the 8×10^{-4} to 9×10^{-4} S/cm range.

CONCLUSIONS

Nanocomposites based on P(4-BAN) and P(ANI-*co*-4-BAN) with cupper-montmorillonite were synthesized by in situ polymerization in the presence of ammonium persulfate is an oxidant. The formation of nanocomposites was confirmed by FTIR, UV–Vis and XRD spectroscopy. The electrical conductivity of the copolymers at room temperature depends on their chemical composition.

Table 3. Peak maximum and *d*-spacing of the nanocomposites intercalated into M-Cu^{2+}

Samples	Peak maximum $2\theta_{max}$, deg	Basal spacing $d(001)$, Å	Interlayer spacing Δd, Å
M-Cu^{2+}	6.71	12.7960	–
P(4-BAN)/M-Cu^{2+}	6.18	14.5695	1.7735
P(ANI-*co*-4BAN)/M-Cu^{2+} (20/80)	5.70	15.0980	0.5285
P(ANI-*co*-4BAN)/M-Cu^{2+} (80/20)	5.73	15.2324	0.2244
P(ANI-*co*-4BAN)/M-Cu^{2+} (50/50)	5.86	15.3081	0.0757

Table 4. Electrical conductivities of polymers/M-Cu^{2+} nanocomposites

Samples	Conductivity, S/cm
M-Cu^{2+}	0.12×10^{-6}
P(4-BAN)/M-Cu^{2+}	8.81×10^{-5}
P(ANI-*co*-4-BAN)/M-Cu^{2+} (20/80)	8.37×10^{-4}
P(ANI-*co*-4-BAN)/M-Cu^{2+} (50/50)	8.92×10^{-4}
P(ANI-*co*-4-BAN)/M-Cu^{2+} (80/20)	9.13×10^{-4}

CONFLICT OF INTEREST

The authors declare that they have no conflicts of interest.

REFERENCES

1. H. Karami, M. F. Mousavi, and M. Shamsipur, J. Power Sources **117**, 255 (2003).
2. C. Y. Lee, H. G. Song, K. S. Jang, E. J. Oh, A. J. Epstein, and J. Joo, Synth. Met. **102**, 1346 (1999).
3. P. J. Alet, S. Palacin, P. I. C. Roca, B. Kalache, M. Firon, and R. De Bettignies, Eur. Phys. J.: Appl. Phys. **36**, 231234 (2006).
4. A. J. McEvoy, M. Gratzel, H. Wittkopf, D. Jestel, and J. Benemann, in *Proceedings of IEEE First World Conference on Photovoltaic Energy Conversion, Waikoloa, HI, USA, 1994* (IEEE Service Center, Piscataway, 1994), p. 178.
5. E. L. Williams, G. E. Jabbour, Q. Wang, S. E. Shaheen, D. S. Ginley, and E. A. Schiff, Appl. Phys. Lett. **87**, 1 (2005).
6. E. W. Paul, A. J. Ricco, and M. S. Wrighton, J. Phys. Chem. **89**, 1441 (1985).
7. S. A. Chen and Y. Fang, Synth. Met. **60**, 215 (1993).
8. S.Virji, J. Huang, R. B. Kaner, and B. H. Weiller, Nano Lett. **4**, 491 (2004).
9. J. X. Huang, S. Virji, B. H. Weiller, and R. B. Kaner, J. Am. Chem. Soc. **125**, 314 (2003).
10. G. Alici, G. M. Spinks, J. D. Madden, Y. Z. Wu, and G. G. Wallace, IEEE/ASME Trans. Mechatronics **13**, 187 (2008).
11. H. Peng, L. Zhang, C. Soeller, and J. Travas-Sejdic, Biomaterials **30**, 2132 (2009).
12. F. Larbi, A. Belfedal, J. Sib, Y. Bouizem, L. Chahed, and A. Amaral, J. Mod. Phys. **2**, 1030 (2011).
13. A. Belfedal, Y. Bouizem, J. Sib, and L. Chahed, J. Non-Cryst. Solids **358**, 1404 (2012).
14. J. Prokes and J. Stejskal, Polym. Degrad. Stab. **86**, 187 (2004).
15. H. L. Wang, R. J. Romero, B. R. Mattes, Y. T. Zhu, and M. J. Winokur, J. Polym. Sci., Part B: Polym. Phys. **38**, 194 (2000).
16. J. Joo, V. N. Prigodin, Y. G. Min, A. G. MacDiarmid, and A. J. Epstein, Phys. Rev. B: Condens. Matter Mater. Phys. **50**, 12226 (1994).
17. A. G. MacDiarmid, Angew. Chem., Int. Ed. **40**, 2581 (2001).
18. G. A. Snook, P. Kao, and A. S. Best, J. Power Sources **196**, 1 (2011).
19. S. I. A. Razak, N. H. M. Sharif, and N. H. M. Nayan, Fibers Polym. **15**, 1107 (2014).
20. D. Li, J. Huang, and R. B. Kaner, Acc. Chem. Res. **42**, 135 (2009).
21. A. M. Youssef, M. A. El-Samahy, and M. Abdel Rehim, Carbohydr. Polym. **89**, 1027 (2012).
22. A. M. Youssef, M. A. El-samahy, M. Elsakawy, and S. Kamel, Carbohydr. Polym. **90**, 1003 (2012).
23. A. Haroun and A. M. Youssef, Synth. Met. **161**, 2063 (2011).
24. M. A. Abd El-Ghaffar, N. A. Mohamed, A. A. Ghoneim, and K. A. Shaffei, Polym.-Plast. Technol. Eng. **45**, 1327(2006).
25. A. A. Wazzan, M. N. Ismail, M. A. Abd El-Ghaffar, Int. J. Polym. Anal. Charact. **10**, 57 (2005).
26. M. N. Ismail, M. S. Ibrahim, and M. A. Abd El-Ghaffar, Polym. Degrad. Stab. **62**, 337 (1998).
27. J. C. Chiang and A. G. MacDiarmid, Synth. Met. **13**, 193 (1986).
28. C. Barbero, J. J. Silber, and L. Sereno, J. Electrochem. **263**, 333 (1989).
29. C. Bouabida, A. Yahiaoui, A. Hachemaoui, and A. M. Benkouider, J. Mater. Environ. Sci. **7**, 4129 (2016).
30. I. Tiffour, S. Bassaid, A. Dehbi, A. Belfedal, A-H-I. Mourad, and A. Zeinert, Surf. Rev. Lett. **26**, 1850127 (2019).
31. I. Tiffour, A. Dehbi, A-H-I. Mourad, and A. Belfedal, Mater. Chem. Phys. **178**, 49 (2016).
32. H. Gherrass, A. Hachemaoui, A. Yahiaoui, A. Belfadel, A. Dehbi and A-H-I. Mourad, J. Semicond. **39**, 102001 (2018).
33. H. Gherras, A. Yahiaoui, A. Hachemaoui, A. Belfedal, A. Dehbi, and A. Zeinert, Polym. Polym. Compos. (2019). https://doi.org/10.1177/0967391119872876
34. A. L. Sharma, Thin Solid Films **517**, 3350 (2009).
35. K. Samrana, A. Shahzada, P. Jiri, P. Josef, and M. J. Yyogesh, J. Mater. Sci. **47**, 420 (2012).
36. M. A. Abd El-Ghaffar, A. M. Youssef, and A. A. Abd El-Hakim, Arabian J. Chem. **8**, 771 (2015).
37. D. Lee, S. H. Lee, K. Char, and J. Kim, Macromol. Rapid Commun. **21**,1136 (2000).